

# Conformational Structure of the MOG-Derived Peptide 101–108 in Solution

Carlo Guardiani,<sup>1</sup> Simone Marsili,<sup>2</sup> Stefania Marchetti,<sup>3</sup> Cecilia Gambi,<sup>3</sup>  
Piero Procacci,<sup>1,2</sup> Roberto Livi<sup>3</sup>

<sup>1</sup>Centro Interdipartimentale per lo Studio delle Dinamiche Complesse (CSDC), Università di Firenze, Italy

<sup>2</sup>Dipartimento di Chimica, Università di Firenze, Italy

<sup>3</sup>Centro Interdipartimentale per lo Studio delle Dinamiche Complesse (CSDC), and Dipartimento di Fisica, Università di Firenze, Italy

Received 3 March 2010; revised 20 May 2010; accepted 1 June 2010

Published online 14 June 2010 in Wiley Online Library (wileyonlinelibrary.com). DOI 10.1002/bip.21510

## ABSTRACT:

One of the most important targets in the autoimmune attack in experimental autoimmune encephalomyelitis is the myelin oligodendrocyte glycoprotein (MOG). The complex with demyelinating 8-18C5 antibody was recently resolved by X-ray crystallography, showing a remarkable adhesion of the 101–108 MOG subsequence to the heavy chain of the autoantibody. In this study, we have determined, using replica exchange molecular dynamics methods, the structure of the MOG-derived peptide 101–108 in solution at ambient conditions. According to the simulation, the peptide exhibits, with significant probability, a distorted  $\beta$ -turn structure highly similar to that of the corresponding subsequence in the crystal in complex with 8-18C5 antibody. Such results are found to be fully consistent with circular dichroism spectra of the peptide in solution, suggesting the use of the MOG-derived 101–108 peptide as a potential lead compound for designing decoy targets for the autoimmune attack in multiple sclerosis. © 2010 Wiley Periodicals, Inc. *Biopolymers (Pept Sci)* 96: 245–251, 2011.

**Keywords:** myelin oligodendrocyte glycoprotein; autoimmune attack; circular dichroism spectroscopy; replica exchange method; conformational distribution of peptides in solution

This article was originally published online as an accepted preprint. The “Published Online” date corresponds to the preprint version. You can request a copy of the preprint by emailing the Biopolymers editorial office at [biopolymers@wiley.com](mailto:biopolymers@wiley.com)

## INTRODUCTION

Multiple sclerosis (MS) is a chronic inflammatory disease of the central nervous system. Although the cause of MS is still uncertain, many findings<sup>1,2</sup> point toward an ongoing autoimmune response to myelin antigens. One of the most important target in the autoimmune attack in experimental autoimmune encephalomyelitis, and possibly in MS, is the myelin oligodendrocyte glycoprotein (MOG). In the recent past, a series of experimental studies<sup>3,4</sup> showed that MOG-specific monoclonal antibodies were unable to recognize a panel of overlapping MOG-derived 15-mer and 25-mer peptides, leading to the conclusion that MOG antibodies recognize only discontinuous epitopes. On the other hand, the structure of the extracellular domain of MOG in complex with the demyelinating 8-18C5 antibody was recently resolved by X-ray crystallography,<sup>5</sup> showing that the discontinuous epitope, composed of the N-terminus, the three upper loops, and two amino acids of the CC' loop, is actually dominated by the FG loop and the flanking G-strand amino acids (residues 101–108). These findings suggest that a MOG-derived fragment as short as the linear 101–108 subsequence, that forms 10 of the 12 intermolecular hydrogen bonds and provides 65% of the total contact area of the MOG/8-18C5 complex, may be used as a blocking agent of the 8-18C5 autoantibody. The importance of MOG subsequence 101–108 has been recently confirmed in Ref. 6 where the two central amino acids His103 and Ser104 of the FG

Correspondence to: Piero Procacci; e-mail: [procacci@chim.unifi.it](mailto:procacci@chim.unifi.it)  
© 2010 Wiley Periodicals, Inc.

loop of MOG (that includes the sequence 101–108) were mutated to determine their importance in the polyclonal Ab response to MOG.<sup>6</sup> Mutation of these two residues reduced binding of a panel of eight demyelinating conformation-dependent mAbs to about 20% compared with binding to wild-type MOG.

To the light of these considerations, the question of the mean structural conformation of MOG peptides depending on their size becomes therefore central in the quest for peptide-based diagnostic or therapeutic agents interacting with MOG-specific monoclonal antibodies. To this regard, the small 101–108 MOG peptide, unlike the larger 15-mer and 25-mer, may be capable of spanning in solution a rather large portion of the accessible conformational space, possibly sampling with significant probability structures that are similar to the structure of 101–108 subsequence in the MOG/8-18C5 complex, thus enabling it to act as a potential decoy target for the autoimmune attack in MS.<sup>7</sup>

Based on the above working hypothesis, the present study is aimed at determining the structural properties of the 101–108 MOG-derived peptide in solution using state of the art computational techniques, validated by experimental data. To this end, we performed molecular dynamics (MD) simulation at the atomistic level of the solvated 101–108 peptide in explicit solvent using the well-established Amber ff199sb force field<sup>8–10</sup> and enhanced sampling techniques. In particular, the MD runs were performed using the replica-exchange<sup>11,12</sup> method to assure a complete sampling of the conformational space of the peptide at ambient conditions. To determine the structural details of the conformational distribution of the peptide in solution, the resulting MD trajectories were analyzed through clustering analysis based on the quality threshold criterion<sup>13</sup> and the peptide conformational pattern was classified according to the dictionary of protein secondary structure (DSSP).<sup>14</sup> From the experimental standpoint, the interpretation of NMR data on small highly flexible peptides is a notoriously contentious task since torsions about chemical bonds (typically occurring on a ns timescale) cause most NMR parameters to be averaged out rather giving a superposition of values as in, for example, optical spectroscopy.<sup>15–18</sup> In this study, we have used circular dichroism (CD) absorption that can give only a coarse grain picture of the structural properties of the peptide. Unlike NMR, however, CD absorption does indeed give superposition of signals arising from different structures and may thus readily provide a reliable estimate of the equilibrium fraction of the 101–108 peptide, that is, in the  $\alpha$ -helix conformation, the  $\beta$  conformation, or random coil, no matter what how fast such structures are interconverting.

The simulation results, consistently with CD measurements, show that the peptide is found with significant proba-

bility in bent of  $\beta$ -turn conformations that are similar (in terms of root mean square displacement (RMSD) metric) to the X-ray resolved structure of the 101–108 MOG subsequence in complex with 8-18C5 antibody. The presence of a relevant fraction of  $\beta$ -turn crystal-like structures in solution for the MOG-derived 101–108 is important, suggesting the possibility of using this peptide (or modification of it enhancing the  $\beta$ -turn stability) as a potential agent for the MOG-specific autoantibody inhibition.

This article is organized as follows: in Section 2, we provide a review of the experimental and computational techniques used throughout the article. In section 3, we present the simulation results obtained for the conformational distribution of the MOG-derived 101–108 in solution along with CD spectra. Final remarks and future perspectives are given in Section 4.

## MATERIALS AND METHODS

### MD Simulation

Explicit solvent simulations of the peptide MOG 101–108 have been performed using an in-house version of the program ORAC,<sup>19,20</sup> the Amber (ff99SB)<sup>9</sup> force field, and the TIP3P model water.<sup>21</sup> The performance of ff99SB/TIP3P in reproducing experimentally derived order parameters in small peptides in solution has been recently found among the best of currently available models.<sup>10</sup> The 101–108 fragment of MOG<sup>1gd</sup> was excised from chain *J* of the complex of this protein with the Fab fragment of the antibody 8-18C5 (PDB-ID: 1PKQ) of the Brookhaven Protein Data Bank.<sup>22</sup> The peptide was then solvated by 871 water molecules in a rhombic dodecahedron box with periodic boundary conditions. The system was initially equilibrated during a 50 ps NPT simulation at  $T = 310$  K and  $P = 1$  atm, where constant pressure was obtained using a modification of the Parrinello-Rahman Lagrangian<sup>23</sup> and temperature control was achieved using a Nosé thermostat.<sup>24</sup> The last configuration obtained from this simulation was used as a starting point for the replica exchange molecular dynamics (REMD) simulations.

The Hamiltonian replica exchange method (REM)<sup>25</sup> implementation of the REM algorithm was adopted in which the replicas of the system differ in their potential energy function  $V$ . In the Hamiltonian REM formalism, the potential of the  $i$ th replica is given by  $V_i = c_i V_0$ , where  $V_0$  is the original potential of the system and  $c_i$  is a multiplicative factor that varies with the replica number. In a canonical simulation, a configuration  $x$  is sampled from the  $i$ th replica with a probability  $P(x) \propto \exp(-V_i(x)/k_B T_0) = \exp(-c_i V_0/k_B T_i)$ . Potential scaling is thus thermodynamically equivalent to simulating the system at an effective temperature  $T_i = T_0/c_i$ . The multiplicative factors were chosen such that the effective temperatures of 56 replicas are distributed over the temperature range from 310.0 to 1033 K with temperature progression according to scheme given in Ref. 25. Replica exchanges are (on average) accepted with a 30% probability. Each replica was equilibrated with a different potential  $V_i$  for 50 ps in the NVT ensemble. Then, exchanges were attempted every 360 fs, leading to an average time of  $\sim 1.2$  ps between two consecutive accepted exchanges. The simulations reached a total simulation time of 840 ns.

The Ewald method with the smooth particle mesh algorithm<sup>26</sup> was used to compute electrostatic interactions. The grid spacing in each dimension of the direct lattice was  $\sim 1.2$  Å, whereas the Ewald convergence parameter was set to  $0.43$  Å<sup>-1</sup>. Electroneutrality was enforced using a uniform positive charge density background equalizing the  $-2$  e excess negative charge on the peptide. A multiple time-step r-RESPA algorithm<sup>27,28</sup> with a potential subdivision specifically tuned for proteins<sup>23,29,19</sup> was used for integrating the equations of motion.

### CD Measurements

The 101–108 MOG peptide was synthesized and purified by Epsi-Kem SRL (Via Ugo Schiff 6, Sesto Fiorentino, 50019 Italy). The sample purity degree, as declared by the provider, is >95%. The molecular weight is 1064 Da. For the CD spectroscopy measurements, a stock solution of 101–108 MOG peptide was prepared by dissolving 2 mg of peptide in 1 ml of Milli-Q water. After, to obtain a final solution concentration of 0.2 mg/ml, appropriate aliquots of this solution were diluted by adding Milli-Q water. The exact solution pH was then monitored with Methohm glass electrode PH-207 and adjusted by adding a very small amount of NaOH to samples. All CD spectra have been collected using a J-715 Jasco spectropolarimeter equipped with a water bath to control the temperature. Samples were inserted into Hellma quartz cylindrical cells with 0.1-cm-path length. Prior to perform the measurements, the cuvette containing the peptide solution was equilibrated at the required temperature for 30 min. Spectra were the average of six scans performed in the range from 260 to 190 nm at 20 nm/min of scanning speed, each with a bandwidth set at 2 nm at the temperature of 310 K. The baseline correction was performed by subtracting the corresponding blank spectra. Although spectra were recorded in the 260–190 nm range, data below 195 nm were not always reliable due to the strong interferences of the solvent at these wavelengths. The observed ellipticity was then converted into mean residue weight ellipticity ( $[T]/\text{deg cm}^2 \text{ dmol}^{-1}$ ) that is normalized for path length and dichroic chromophore concentration. Smoothing of the curves, using a mild function that increased the signal-to-noise ratio without altering the shape of the spectra, was applied using the Jasco J-715 program. Superimposition of the smoothed spectra with the raw curve was performed each time to check for artifacts. The far-UV CD spectra were analyzed on DICHROWEB website,<sup>30–32</sup> using CDSSTR<sup>33,34</sup> algorithms, with the basis set including CD spectra of 48 globular proteins of solved structures.<sup>34,35</sup>

## RESULTS AND DISCUSSION

In the explicit solvent simulation, a total of 7905 structures were sampled at  $T = 310$  K during the REMD simulations. A subset of 905 structures, corresponding to the initial 11.5% of the simulation, were discarded to make sure to use only structures decorrelated from the initial, crystallographic conformation.

As mentioned in the Introduction, our working hypothesis is that there exists a high fraction of crystal-like structures in the equilibrium population (possibly allowing<sup>7</sup> the MOG-derived peptide 101–108 to recognize the binding pocket of

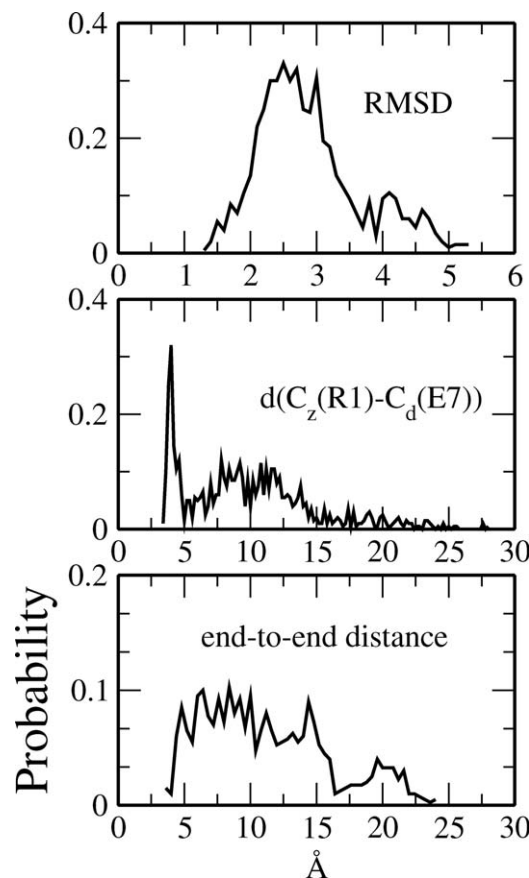


**FIGURE 1** Structural data obtained from the replica exchange simulation of the MOG-derived peptide 101–108 in solution at  $T = 310$  K and  $P = 1$  atm. Top: Distribution of the  $\text{RMSD}_{\text{backb}}$  from the crystal structure of fragment MOG 101–108 (calculated using the coordinates of the backbone atoms only). Center panel: Distribution of the distances between  $C_{\alpha}$  of Arg101 and  $C_{\delta}$  of Glu107. Right panel: Distributions of the end-to-end distance.

the 8-18C5 antibody). The thermodynamical relevance of crystal-like structures is fully confirmed in Figure 1 where we show the probability distribution of the RMSD of the MOG-derived peptide 101–108 in solution from the structure of the 101–108 subsequence of extracellular domain of MOG in complex with a Fab derived from the demyelinating mAb 8-18C5. The  $\text{RMSD}_{\text{backb}}$  distributions shown in Figure 1 reveals in fact that the RMSD distance from the crystal structure features a marked peak below 3 Å, with a fraction of about 38% of the sampled structures bearing an RMSD distance from the crystal of less than 2.5 Å. These data are particularly significant since the MOG/8-18C5 complex was resolved at a resolution of 3 Å.<sup>5</sup>

Figure 1 also shows the histogram of distances between  $C_{\alpha}$  of Arg101 and  $C_{\delta}$  of Glu107. Such a probability distribution exhibits a narrow peak at 5 Å corresponding to structures where the salt bridge between Arg101 and Glu107 plays a key

**Table I** Data From Clustering Analysis Based on the RMSD (Backbone Atoms Only) of the Peptide From the Crystal Structure of the Corresponding Subsequence 101–108 in the MOG/8-18C5 Antibody Complex

<i>i</i>	<i>p</i>	<i>d</i> <sub>cryst</sub>	<i>d</i> <sub>r-e</sub>	<i>d</i> <sub>end-end</sub>	<i>r</i> <sub>gyr</sub>
1	0.202	2.56	8.93	8.39	5.89
2	0.153	2.68	7.39	6.91	5.79
3	0.136	2.45	7.04	14.59	6.7
4	0.091	4.52	19.14	21.11	8.17
5	0.087	2.63	9.53	12.11	6.34
6	0.056	2.14	8.42	7.55	6.09
7	0.034	2.85	6.61	11.89	5.97
8	0.033	2.90	10.11	8.52	6.01
9	0.033	4.36	17.14	18.84	7.79
10	0.030	3.27	12.74	14.82	6.90
11	0.028	3.81	10.51	12.23	6.19
12	0.021	3.46	9.37	5.96	5.93
13	0.020	3.99	12.43	15.01	6.22
14	0.017	2.90	10.87	13.88	6.59
15	0.015	3.38	6.92	9.24	5.88
16	0.009	3.20	11.86	15.35	6.71
17	0.006	2.95	11.19	11.55	6.09
18	0.006	4.19	15.91	19.55	7.60
19	0.006	2.07	7.50	7.92	6.11
20	0.005	3.43	9.26	10.56	6.09
21	0.005	3.56	10.15	12.21	5.93
22	0.003	2.87	12.33	4.31	5.72
23	0.002	3.51	13.08	7.93	6.05
24	0.001	4.39	4.99	12.13	5.83
25	0.001	3.10	14.71	14.71	6.18

Data were obtained from the REMD simulation of MOG-derived peptide 101–108 at  $T = 310$  K and  $P = 1$  atm in explicit solvent.  $p \equiv N_i/N_{\text{tot}}$  is fractional population of the cluster *i*,  $d_{\text{cryst}}$  is its average RMSD from the crystal structure,  $d_{\text{r-e}}$  is the average distance between the  $C_\alpha$  carbon of Arg101 and the  $C_\beta$  carbon of Glu107 in the cluster, and  $d_{\text{end-end}}$ ,  $r_{\text{gyr}}$  are its mean end-to-end distance and radius of gyration, respectively.

role for stability, and a broad distribution at higher distances where other contacts are more relevant. The end-to-end distance distribution (Figure 1, bottom panel) acts as an overall indicator of the attraction between the N- and C-terminus and, indirectly, of the stability of hairpin-like structure. The histogram of this parameter indicates that a relevant fraction of the conformational states of the peptide has end-to-end distances below 10 Å, a result that appears to be consistent with a significant incidence of bent, hairpin-like structures.

To obtain a more detailed information on the nature of the conformational space of the peptide in solution, the resulting conformational population of the 101–108 peptide was clustered using a quality threshold algorithm<sup>13</sup> with a  $\text{RMSD}_{\text{backb}}$  cutoff of 3.0 Å. The population obtained from the explicit solvent simulation on the target replica was divided into 25 clusters. Data on the clustering analysis are collected in Table I.

In Figure 2, we report the structures that are found closer to the centroid of the four most populated clusters. Three of these representative structures have RMSD from the crystal structure that are below 3 Å (see also Table I). When the representative structure of cluster 1 is superposed to the MOG 101–108 crystal so as to minimize the distance between backbone atoms, we obtain an  $\text{RMSD}_{\text{backb}}$  of only 2.07 Å. It can be noticed that in the representative structure of cluster 1, the  $\beta$ -turn is kinked yielding two slightly divaricated branches. This deformation allows the side chain of Arg101 to adopt a suitable orientation so as to establish hydrogen bonds with the carboxy-terminal group and with the side chain of Glu107, providing therefore an energetic basis for the clustering of  $\beta$ -turn structures. The representative set of cluster 2 is still bent and still quite similar to the structure found in the most populated cluster, yielding, and RMSD of 2.59 Å from the crystal structure. In the third cluster, the hairpin is still slightly divaricated and the carboxy-terminal  $\beta$ -strand appears to be undulate, but the structure is indeed very similar to the crystal with  $\text{RMSD}_{\text{backb}}$  of only 1.73 Å. Cluster 4, conversely, is populated by extended conformations that are clearly not crystal

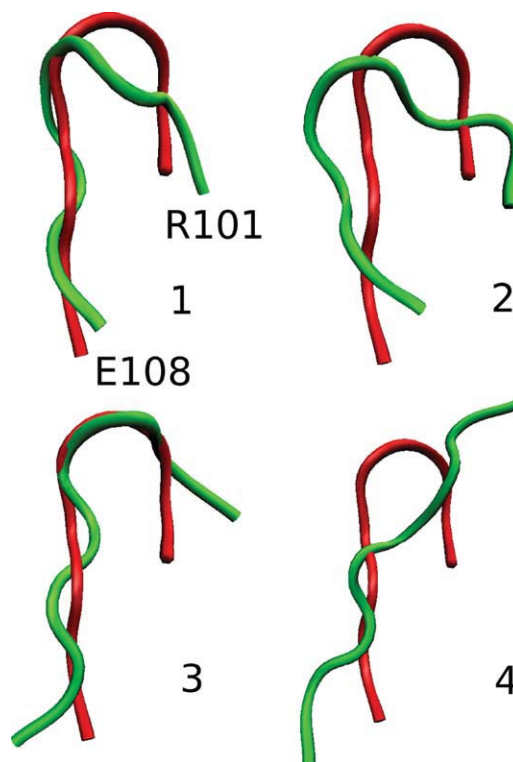


**FIGURE 2** Comparison of the structures of the centroid of the four most populated cluster (see also Table I) obtained from the REMD simulation of peptide MOG 101–108 with the structure of the MOG subsequence 101–108 in the crystal. The cluster structures (in green) are superposed to the crystal fragment (in red) so as to minimize the distance between backbone atoms.



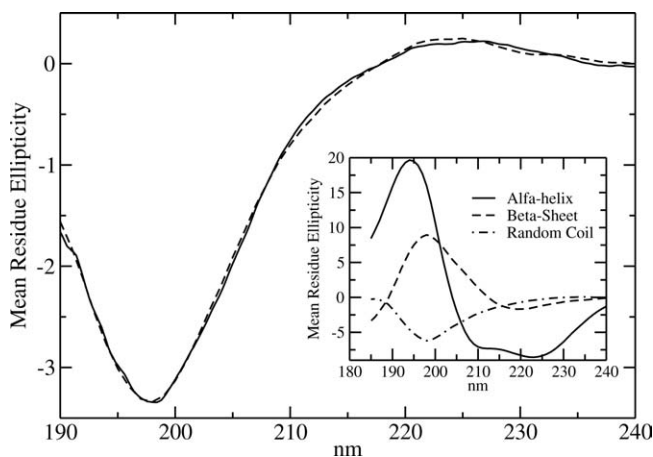


**FIGURE 3** Circular dichroism absorption spectrum of the MOG-derived peptide 101–108 in aqueous solution at pH 7 and at normal conditions. Ellipticity is expressed in  $\text{deg } 10^{-3} \text{ cm}^2 \text{ dmol}^{-1}$ . The dashed line is a fit obtained using the DICHROWEB platform<sup>30</sup> with a basis set including CD spectra of 48 globular proteins of solved structure. Results of the fit are: 0.0 regular helix; 0.06 distorted helix; 0.25 regular  $\beta$ -strand; 0.12 distorted  $\beta$  structure; 0.22 turn; and 0.35 unordered structure. In the inset, the pure CD spectra of  $\alpha$ -helical,  $\beta$ -sheet, and random coil (including turn) obtained by performing the Penrose pseudoinverse of the weight  $50 \times 3$  matrix taken from the reference set of 50 globular proteins (database labeled SMP50 in the CDPRO software package; see Ref. 36 and reference therein).

like with the RMSD distance between the centroid of this cluster and the crystal structure being 4.68 Å.

On the overall, the simulation data indicate that a significant fraction (about 50%) of the equilibrium population of the 101–108 peptide is characterized by bent structures similar to the  $\beta$ -turn structure of the 101–108 subsequence observed in the crystal MOG/8-18C5 complex.

In Figure 3, we report the CD spectrum of the peptide in solution at ambient condition and at pH = 7 along with a fit done using a data set of 48 globular proteins and using the CDSSTR analysis program at the DICHROWEB<sup>30</sup> website. The fitted spectrum shows a typical pattern of a random coil unordered structure (see the inset in Figure 3) with negative and positive mean residue ellipticity below and above 210 nm, respectively, indicating that the peptide must have a rather flexible structure in solution. The CD spectrum, according to the CDSSTR program, bears a significant contribution from  $\beta$ -like structures (about 50% on the overall) and virtually no contribution from  $\alpha$ -helical structures. Such results appear to be consistent with the results obtained from the clustering analysis on the simulation data (see Section 1), where about one half of the structures were found in clusters characterized by a bent or  $\beta$ -like structures).

As shown in Figure 4, the basic structural features of the peptide appear to be preserved also in acid or basic solution, with all CD spectra invariably exhibiting in the pH interval 5.5–9.0, the typical random coil pattern. The populations of the secondary structures obtained through the CDSSTR analysis at various pH do not differ much from that obtained at pH = 7, yielding a  $\beta$  content always around 45–50% and a nonsignificant contribution from helix-like structure in both acid and basic solution. These results suggest that the conformational distribution of the 101–108 peptide must be quite insensitive to the protonation state of Asp102, His103, Glu107, and Glu108. The CD spectra, although valuable, give only coarse structural information with no clear indications neither on the stability nor on the extensions and characteristics of the  $\beta$ -structure content. As a matter of fact, due to the nonrigidity of the peptide in solution, the distinction between  $\beta$ -turn,  $\beta$ -sheet, or distorted  $\beta$ -strands based on the highly undetermined system of the CD data alone is a rather risky operation.<sup>37</sup> Given the overall consistency between experiment and simulation data, we could then use the latter to shed some further light on the dynamical distribution of secondary structure motifs and on their precise structural nature. To this aim, we have done a DSSP<sup>14</sup> analysis in the target replica for 7000 conformations evenly distributed in the 15-ns time span of the explicit solvent simulation of the peptide 101–108. The secondary structure for each of the 7000 structures is assigned according to the convention provided in the DSSP program<sup>14</sup> and the results of such analysis are conveyed in Table II. The DSSP analysis confirms, as seen in the CD spectrum, that the helical content of the peptide in solution is negligible with an overall percentage of G, I, and H helix not exceeding 2% (5% in the CD analysis). The over-

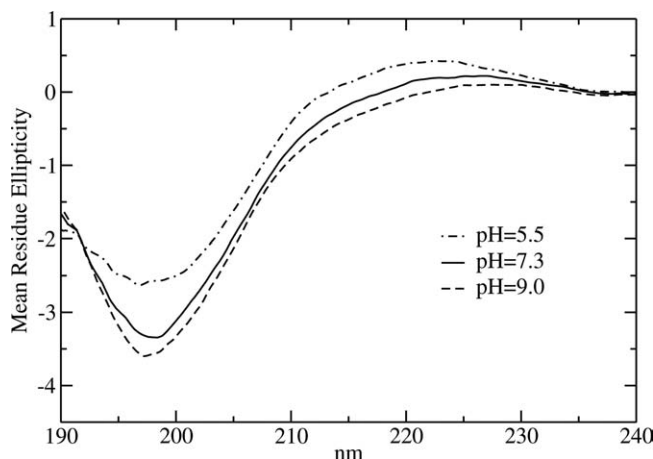


**FIGURE 4** Circular dichroism absorption spectrum of the MOG-derived peptide 101–108 in aqueous solution at various pH and ambient conditions. Ellipticity is expressed in  $\text{deg } 10^{-3} \text{ cm}^2 \text{ dmol}^{-1}$ .

**Table II** Secondary Structure Assignment of 7000 Configurations of the MOG-Derived Peptide 101–108 Sampled From A 15 ns REMD Simulation At Ambient Conditions

S	B	T	E	H	G	I	n.a.	
R101	0.000	0.000	0.000	0.000	0.000	0.000	0.000	1.000
D102	0.000	0.016	0.010	0.000	0.001	0.002	0.000	0.970
H103	0.324	0.003	0.307	0.000	0.003	0.015	0.000	0.348
S104	0.358	0.000	0.411	0.000	0.004	0.027	0.000	0.200
Y105	0.387	0.008	0.249	0.000	0.004	0.028	0.000	0.323
Q106	0.239	0.008	0.064	0.000	0.003	0.017	0.000	0.669
E107	0.000	0.003	0.027	0.000	0.001	0.003	0.000	0.966
E108	0.000	0.000	0.000	0.000	0.000	0.000	0.000	1.000

Residues from 101 to 108 are indicated with the one letter code. For each configuration of the peptide, secondary structure was determined using the DSSP program.<sup>14</sup> On each row (residue), the fraction of secondary structures found in the simulation is reported. The secondary structures are defined according to the DSSP convention: Entry S: bend residue; Entry B: residue on isolated  $\beta$  bridge; Entry T: hydrogen-bonded turn; Entry E: residue in extended  $\beta$  bridge; Entry H: residue in  $\alpha$ -helix; Entry G: residue in  $\pi$ -helix; Entry I: residue in 3–10 helix; Entry n.a.: none of the above rules pertains.

all percentage of hydrogen bond turn structures (T) is about 13% (against the 20% found in the CD spectrum). While expectedly in such a small peptide, an insignificant fraction of residues can be assigned to either extended or isolated  $\beta$  bridge (E or B) about 16% of the residues are found in bent conformations (S) with angles between the vector from  $C_{\alpha}(i)$  to  $C_{\alpha}(i+2)$  and the vector from  $C_{\alpha}(i-2)$  to  $C_{\alpha}(i)$  less than  $70^{\circ}$ . The sum of  $\beta$ -like or turn/bent structures (thus including the S motif) amounts to about 30%, in semiquantitative agreement with the CDSSTR analysis on the CD spectrum. The remainder of the residues (about 70%) cannot be assigned to any of the above DSSP motifs, and could generically be classified as random coil, again in semiquantitative agreement with the CD analysis. We also remark that the DSSP data for the explicit solvent simulations are consistent with the corresponding data from clustering analysis (see Table I) according to which a fraction of about 50% of the equilibrium conformations belongs to clusters in bent or  $\beta$ -turn structures.

The distribution of the secondary structure along the peptide primary chain, as found in MD simulations, shows that the bend (S) or turn (T) structures overwhelmingly occur within the His103–Tyr105 subsequence, consistently with the clustering analysis (see Section 3 and Figure 2) whereby the peptide chain is likely to bend at the level of His103–Tyr105 and exactly as it happens in the 101–108 subsequence of the X-ray structure of the MOG protein in complex with a Fab derived from the demyelinating mAb 8-18C5.

## CONCLUSIONS

The present study was aimed at determining the structure of the MOG-derived peptide 101–108 combining accurate simulation data at the atomistic level using REMD technology for enhanced sampling supported by CD measurements. Simulation data indicate that the peptide adopts a bent con-

formation with a significant probability. These results are found to be consistent with the CD spectrum of the peptide in solution. Clustering analysis and DSSP assignment show that an irregular kinked turn is likely to occur in the subsequence 103–105. The MD simulation data indicate that the relative abundance of such bent structures in the solvated peptide is due to electrostatic stabilization between the two terminal branches of the turn (i.e., Arg101–Glu107 or Arg101–Glu108 interactions). Furthermore, the CD spectrum shows that the incidence of  $\beta$ -like structures does not change appreciably with varying pH conditions. Our structural analysis based on MD and CD data may serve as a basis for the interpretation<sup>17,18</sup> of possible ROESY and NOESY NMR experiments of MOG-derived peptides in solution, and at the same time can be further validated by these studies. Given the fact that in the crystal structure of the MOG/8-18C5 complex, a regular  $\beta$ -turn is observed in the segment His103–Tyr105, the pH resistant capability of the MOG-derived peptide 101–108 of assuming in solution configurations matching those observed in the MOG/8-18C5 complex could in principle provide a biomimetic route for designing molecules for early diagnosis and/or therapeutic agent for MS.

The authors thank Regione Toscana for financial support (“Ricerca regionale in materia di salute”, D.D. n. 3242 del 30/06/09).

## REFERENCES

1. Linington, E.; Berger, T.; Perry, L.; Weerth, D. H.-S.; Zhang, Y.; Lu, H.; Lassmann, H.; Wekerle, H. *Eur J Immunol* 1993, 23, 1364–1372.
2. Zhou, D.; Srivastava, R.; Nessler, S.; Grummel, V.; Sommer, N.; Brück, W.; Hartung, H.; Stadelmann, C.; Hemmer, B. *Proc Natl Acad Sci USA* 2006, 103, 19057–19062.
3. Brehm, U.; Piddlesden, S.; Gardinier, M.; Linington, C. *J Neuroimmunol* 1999, 97, 9–15.

4. Guggenmos, C. H. J.; Brehm, U.; Andersson, M.; Olsson, T.; Reindl, M.; Schneidewind, J.; Zettl, U.; Heidenreich, F.; Berger, T.; Wekerle, H.; Hohlfeld, R.; Linington, C. *J Neuroimmunol* 2001, 114, 220–225.
5. Breithaupt, C.; Schubart, A.; Zander, H.; Skerra, A.; Huber, R.; Linington, C.; Jacob, U. *Proc Natl Acad Sci USA* 2003, 100, 9446–9451.
6. Breithaupt, C.; Schäfer, B.; Pellkofer, H.; Huber, R.; Linington, C.; Jacob, U. *J Immunol* 2008, 181, 1255–1263.
7. Guardiani, C.; Marsili, S.; Procacci, P.; Livi, R. *J Am Chem Soc* 2009, 131, 17176–17184.
8. Case, D. A.; Darden, T.; Cheatham, T.; Simmerling, C.; Wang, J.; Duke, R.; Luo, R.; Merz, K.; Pearlman, D.; Crowley, M.; Walker, R.; Zhang, W.; Wang, B.; Hayik, S.; Roitberg, A.; Seabra, G.; Wong, K.; Paesani, F.; Wu, X.; Brozell, S.; Tsui, V.; Gohlke, H.; Yang, L.; Tan, C.; Mongan, J.; Hornak, V.; Cui, G.; Beroza, P.; Mathews, D.; Schafmeister, C.; Ross, W.; Kollman, P.; AMBER9, University of California, S. Francisco 2006.
9. Hornak, V.; Abel, R.; Okur, A.; Strockbine, B.; Roitberg, A.; Simmerling, C. *Proteins Struct Funct Bioinf* 2006, 65, 712–725.
10. Wickstrom, L.; Okur, A.; Simmerling, C. *Biophys J* 2009, 97, 853–856.
11. Marinari, E.; Parisi, G. *Europhys Lett* 1992, 19, 451–458.
12. Sugita, Y.; Okamoto, Y. *Chem Phys Lett* 1999, 314, 141–151.
13. Heyer, L. J.; Kruglyak, S.; Yoosheph, S. *Genome Res* 1999, 9, 1106–1115.
14. Kabsch, W.; Sander, C. *Biopolymers* 1983, 22, 2567–2637.
15. Lipari, G.; Szabo, A. *J Am Chem Soc* 1892, 104, 4546–4559.
16. Williamson, M. P. In *Spectroscopic Methods and Analyses*; Jones, C.; Mulloy, B.; Thomas, A., Eds.; Humana Press: Totowa, New Jersey, 1993; Chapter 2.
17. Feenstra, K. A.; Peter, C.; Scheek, R. M.; van Gunsteren, W. F.; Mark, A. E. *J Biomol NMR* 2002, 23, 181–194.
18. Fawzi, N. L.; Phillips, A. H.; Ruscio, J. Z.; Doucleff, M.; Wemmer, D. E.; David, E.; Head-Gordon, T. *J Am Chem Soc* 2008, 130, 6145–6158.
19. Procacci, P.; Paci, E.; Darden, T.; Marchi, M. *J Comp Chem* 1997, 18, 1848–1862.
20. Marsili, S.; Signorini, G. F.; Chelli, R.; Marchi, M.; Procacci, P. *J Comp Chem* 2010, 31, 1106–11161.
21. Jorgensen, W. L.; Chandrasekhar, J.; Madura, J.; Impey, R.; Klein, M. *J Chem Phys* 1983, 79, 926–935.
22. Bernstein, F. C.; Koetzle, T.; Williams, G.; Meyer, E., Jr.; Brice, M.; Rodgers, J.; Kennard, O.; Shimanouchi, T.; Tasumi, M. *J Mol Biol* 1977, 112, 535–542.
23. Marchi, M.; Procacci, P. *J Chem Phys* 1998, 109, 5194–5202.
24. Nose, S. *Mol Phys* 1984, 52, 255–268.
25. Fukunishi, H.; Watanabe, O.; Takada, S. *J Chem Phys* 2002, 116, 9058–9067.
26. Essmann, U.; Perera, L.; Berkowitz, M.; Darden, T.; Lee, H.; Pedersen, L. *J Chem Phys* 1995, 103, 8577–8593.
27. Tuckerman, M.; Berne, B. J.; Martyna, G. *J Chem Phys* 1992, 97, 1990–2001.
28. Procacci, P.; Berne, B. J. *Mol Phys* 1994, 83, 255–272.
29. Procacci, P.; Marchi, M. *J Phys Chem* 1996, 100, 10464–10469.
30. Whitmore, L.; Wallace, B. A. *Biopolymers* 2008, 89, 392–400.
31. Whitmore, L.; Wallace, B. A. *Nucleic Acid Res* 2004, 32, W668–W673.
32. Lobley, A.; Whitmore, L.; Wallace, B. A. *Nucleic Acid Res* 2004, 32, W668–W673.
33. Compton, L. A.; Johnson, W. C., Jr. *Anal Biochem* 1986, 155, 155–167.
34. Sreerama, N.; Venyaminov, S. Y.; Woody, R. W. *Anal Biochem* 2000, 287, 243–251.
35. Sreerama, N.; Woody, R. W. *Anal Biochem* 2000, 282, 252–260.
36. Sreerama, N.; Woody, R. *Methods Enzymol* 2004, 383, 318–351.
37. Khrapunov, S. *Anal Biochem* 2009, 389, 174–176.